Electron mobility in modulation-doped heterostructures

W. Walukiewicz,* H. E. Ruda,† J. Lagowski, and H. C. Gatos
Massachusetts Institute of Technology, Cambridge, Massachusetts 02139
(Received 2 April 1984; revised manuscript received 4 June 1984)

A model for electron mobility in a two-dimensional electron gas confined in a triangular well was developed. All major scattering processes—i.e., deformation potential and piezoelectric acoustic, polar optical, ionized impurity, and alloy disorder—were included as well as intrasubband and intersubband scattering. The model is applied to two types of modulation-doped heterostructures, namely GaAs-GaAlAs and $In_{0.53}Ga_{0.47}As$-$Al_{0.52}In_{0.48}As$. In the former case phonons and remote ionized impurities ultimately limit the mobility, whereas in the latter, alloy disorder is a predominant scattering process at low temperatures. The calculated mobilities are in very good agreement with recently reported experimental characteristics for both GaAs-$Ga_{1-x}Al_xAs$ and $In_{0.53}Ga_{0.47}As$-$Al_{0.52}In_{0.48}As$ modulation-doped heterostructures.

I. INTRODUCTION

The advent of modulation- (or selectively-) doped heterostructures (MDH) has prompted a wave of studies, both theoretical and experimental, on the two-dimensional electron gas (2D EG). As MDH with exceedingly high electron mobilities have been obtained, a new challenge associated with the understanding of the transport properties of the 2D EG has emerged.

The concept of separating electrons from their parent donors in semiconducting systems was originally proposed by Esaki and Tsu.[1] However, it was not until molecular-beam epitaxy (MBE) technology was sufficiently developed that such structures were grown.[2] It soon became apparent that these types of structures are the key to a new generation of high-speed semiconductor devices.[3–7]

Many of the studies concerned with electron mobility treated the confining potential as a square well; this treatment is only applicable to multiple-quantum-well structures.[8–11] However, the highest electron mobilities have been observed in single-quantum-well structures, where a triangular potential well is a better suited approximation. The framework for the treatment of two-dimensional electron transport in a triangular well was originally developed for silicon inversion layers.[12–14] This approach was adapted to the treatment of scattering by ionized impurities, by alloy disorder, and by surface roughness in GaAs-$Ga_{1-x}Al_xAs$ MDH.[15] The treatment, however, was limited to intrasubband scattering, and therefore it was not applicable to higher gas densities. The effect of doping of GaAs on the electron mobility in GaAs-$Ga_{1-x}Al_xAs$ heterostructures has been also considered.[16] Since in MDH ionized-impurity scattering is substantially reduced, even at low temperatures electron-phonon interaction constitutes an important mechanism limiting electron mobility. The problem of electron-phonon scattering has been addressed in general terms, and the difficulties a proper description of optical-phonon scattering would entail, especially at higher temperatures, were pointed out.[17,18] Electron mobilities have been also calculated for GaAs-$Ga_{1-x}Al_xAs$ MDH taking phonon scattering into consideration,[19] however, the calculated values are much lower than those reported recently.[20,21] A simplified approach to 2D EG mobility calculations in a triangular well has been carried out by adopting formulas valid for a square well potential and using an effective width taken as the average separation of the electrons from the interface.[22] In addition to these simplifications alloy-disorder scattering was not taken into account.

An important feature of an electron gas confined in a 2D potential well is the quantization of the electron energy in the potential well leading to a splitting of the three-dimensional (3D) conduction band into two-dimensional subbands. The importance of intersubband scattering has been implicated in numerous experimental investigations.[5,6,21,23] To date, however, apart from treatment of the phonon scattering,[17,18] the mobility calculations of 2D EG in MDH have been carried out considering only intrasubband scattering.[22,15]

In this paper we have formulated a model to calculate electron mobilities in 2D EG confined in a triangular well, taking into consideration all major scattering mechanisms, and considering both intrasubband and intersubband scattering.[24] Preliminary results on GaAs-$Ga_{1-x}Al_xAs$ heterostructures have been considered previously.[25] This paper has been structured as follows: In Sec. II we discuss essential features of the MDH used for the confinement of the electron gas. Also, the energetic structure of 2D EG in a triangular well is described. The relaxation times for all the considered scattering processes including intrasubband as well as intersubband transitions are obtained in Sec. III. Results of this section are then applied in Sec. IV to calculate characteristics of the electron mobility for MDH based on various semiconducting systems. The results are compared with published experimental data. Summary and conclusions are given in Sec. V.

II. ELECTRONIC STRUCTURE OF SINGLE QUANTUM WELL

We consider the single quantum well at the interface of two semiconductors of different electron affinities and

band gaps. As shown schematically in Fig. 1, the larger affinity semiconductor ($S1$ at $z \geq 0$) is nominally undoped, while the lower affinity semiconductor ($S2$ at $z<0$) is selectively doped, i.e., it contains the undoped region $-d<z<0$ (commonly referred to as the "spacer") and the region $z \leq -d$ highly doped with shallow donors. As a result of the electron affinity difference, electrons from the donors in $S2$ are transferred to $S1$, and accumulate in the vicinity of the interface; this results in a strong electric field perpendicular to the interface. This field leads to a quantization of the energy band structure: the subband energies and their separation depend on the electric field. In general, the electric field varies with the distance from the interface, and an accurate description of wave functions and eigenvalues would require elaborate numerical calculations. However, it has been found that the single quantum well of the MDH can be effectively approximated by a finite triangular well. In this approach the eigenvalues and wave functions for the ground and first-excited subbands can be expressed in a simple manner, using one independent parameter related to the electric field within the well. For the ground subband (0) and excited subband (1), the wave functions are[14,18]

$$\psi_0(\vec{r},z)=\phi_{k_x,k_y}(r)\chi_0(z)=\phi_{k_x,k_y}\frac{z\exp(-b_0z/2)}{(b_0^3/2)^{1/2}}, \tag{1a}$$

$$\psi_1(\vec{r},z)=\phi_{k_x,k_y}(\vec{r})\chi_1(z)$$
$$=\phi_{k_x,k_y}A(2/b_0^3)^{1/2}z(1-Bz)\exp(-b_1z/2), \tag{1b}$$

where $\phi_{k_x,k_y}(\vec{r})$ is the two-dimensional plane wave

$$A=[3b_1^5b_0^3/4(b_0^2-b_0b_1+b_1^2)]^{1/2}$$

and $B=(b_0+b_1)/6$. The parameters b_0 and b_1 were evaluated by comparing the roots of the wave-functions and their first derivatives for (0) and (1) subbands, given by Eqs. (1a) and (1b) with roots of corresponding wave functions derived from the Airy-function solutions for a triangular well. For a given effective mass of the electron, m^*, there is a relationship between b_0 and b_1. Thus, for GaAs it is found that $b_1 \simeq 0.754 b_0$, which in turn gives the following relationships: $A \simeq 0.47 b_0^3$ and $B \simeq 0.292 b_0$. Therefore, the forms of the wave functions (1a) and (1b) are determined by one parameter, b_0. On the other hand, the parameter b_0 is determined by the electric field within the well, or equivalently, by the electron gas density,

$$b_0 \propto (N_s')^{0.36}. \tag{2}$$

where $N_s'=(N_s+\frac{32}{11}N_{\text{depl}})$, and N_{depl} is the areal concentration of charge in the depleted region of $S1$.

The energies of the (0) and (1) subbands are

$$E_{0,1}(k)=E_{0,1}+\frac{\hbar^2k^2}{2m^*}, \tag{3}$$

where $\vec{k}=(k_x,k_y)$ is a two-dimensional wave vector and $E_{0,1}$ are the energy band minima of the ground (0) and excited (1) subbands, respectively. The total number of electrons in the well per unit area, i.e., the electron-gas density, N_s, is given by the equation,

$$N_s=\frac{m^*}{\pi\hbar^2}\sum_{i=0}^{j_{\max}}[(E_F-E_i)\Theta(E_F-E_i)], \tag{4}$$

where

$$\Theta(E)=\begin{cases}0 \text{ for } E<0,\\ 1 \text{ for } E\geq 0.\end{cases}$$

Equation (4) is used to determine the Fermi wave vector for the electrons in the ground subband.

In our approach the energy separation $\Delta_{10}=E_1-E_0$ depends on the electric field, or equivalently on the parameter, b_0. For example, for the case of GaAs

$$\Delta_{10}=1.23\times10^{-11}b_0^{1.93}\ \text{meV}. \tag{5a}$$

where b_0 is in cm^{-1}. Thus the critical gas density N_s^{crit} at which the Fermi energy E_F reaches the first excited subband is given by

$$\Delta_{10}=E_F^{\text{crit}}=\frac{\pi\hbar^2}{m^*}N_s^{\text{crit}}, \tag{5b}$$

since b_0 can be expressed in terms of N_s in the present model [see Eq. (2)], one has to include only two parameters, N_s and N_s^{crit}, to completely define the system. For a GaAs-$Ga_{1-x}Al_xAs$ heterostructure with $N_{\text{depl}}=5\times10^{10}$ cm^2, $N_s^{\text{crit}}=7.5\times10^{11}$ cm^{-2}, which corresponds to an energy separation of 24 meV, the values of b_0 calculated from Eq. (2) do not differ by more than 20% from values estimated from the self-consistent calculations of Ref. 15.

In equilibrium the transfer electrons from the doped region to the well[15] of the MDH shown in Fig. 1 is governed by the following equation:

$$E_0+E_F=V_0-E_b-\frac{4\pi e^2}{2\epsilon_s}\frac{(N_s+N_{\text{depl}})^2}{N_i^r}$$
$$-\frac{4\pi e^2}{\epsilon_s}(N_s+N_{\text{depl}})d, \tag{6}$$

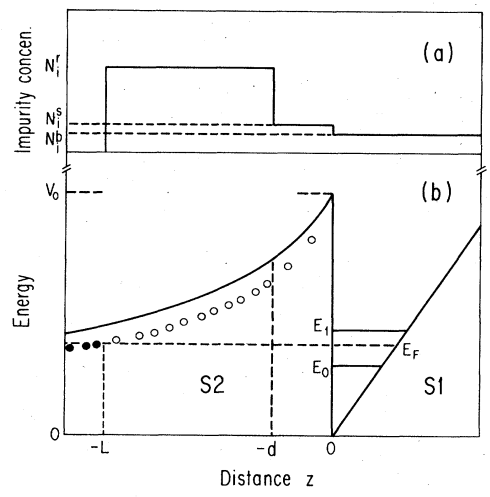

FIG. 1. Schematic representation of (a) the doping profile, and (b) the energy configuration for a single-quantum-well modulation-doped heterostructure; see text.

where V_0 is the conduction band energy offset, E_b is the donor binding energy in the doped part of semiconductor $S2$, ϵ_s is the static dielectric constant, and N_{depl} is the areal concentration of ionized donors in depleted regions of $S1$. The above equation was used to calculate the concentration of ionized remote impurities, N_i^r, as a function of electron-gas density N_s and undoped spacer width d.

III. SCATTERING MECHANISMS

There are certain features which distinguish electron transport in two and three dimensions. For example, in the case of ionized impurities, there are two distinctly different types of scattering in the two-dimensional case: Electrons can be scattered by remote impurities located within the doped region of the $S2$ semiconductor as well as by residual background impurities in the $S1$ semiconductor. Also, there is the possibility of scattering by interface charges, located at the heterojunction interface.

The dominant scattering mechanisms for bulk III-V compounds are now well established.[26] In our calculations of electron mobility in the 2D EG we included all these mechanisms, and in addition included scattering processes unique to the 2D EG structures, as alluded to above. We consider a range of electron-gas densities, which justifies the use of degenerate-electron statistics at temperatures below 60 K. Therefore, the inverse of the total relaxation time $1/\tau_{\text{tot}}$ can be calculated from the sum of the scattering rates for the individual processes:

$$1/\tau_{\text{tot}}=\sum_i 1/\tau_i \ . \tag{7}$$

At higher temperatures, relation (7) may not be valid due to the limited applicability of degenerate statistics, and also of the relaxation-time approximation for the polar-optical-phonon scattering. However, for temperatures higher than 60 K the scattering in 2D EG is dominated by polar scattering. Accordingly, we have calculated this scattering separately using general Fermi-Dirac statistics in a three-dimensional approximation. In our calculations of electron transport, we consider the two lowest subbands (0) and (1). In general, to calculate electron transport in such systems, one must treat the two subbands as coupled through intersubband [(0)→(1)] scattering. For low electron-gas densities, subband (1) is empty, and the conductivity within this subband does not contribute to the total conductivity. The major effect of subband (1) is through the density of the final states available for the scattering of electrons; it increases abruptly when the Fermi energy exceeds the energy separation between two subbands, Δ_{10}. Intersubband scattering would result in an abrupt decrease of the electron mobility for electron concentrations exceeding N_s^{crit}. However, since the actual density-of-states function is broadened, one expects a gradual increase of intersubband scattering for N_s close to N_s^{crit}. We included these effects by considering the broadening to be described by a simple Lorentzian function with energy-independent broadening parameter Γ. The relaxation time for intersubband scattering is then modified in the following way:

$$\left[\frac{1}{\tau_i(E)}\right]_{\text{broad}}=\left[\frac{1}{\tau_i(E)}\right]_{\text{unbroad}}\frac{1}{\pi}\times\left[\frac{\pi}{2}+\tan^{-1}\left[\frac{E-E_1}{\Gamma}\right]\right] . \tag{8}$$

A. Phonon scattering

It has been shown[26] that phonon scattering plays an important role in limiting the electron mobility in III-V semiconducting compounds. The most important phonon scattering processes are (i) deformation potential acoustic, (ii) piezoelectric acoustic, and (iii) polar optical. To calculate the matrix elements for the appropriate scattering process, a quasi-three-dimensional approximation was adopted, in which the perturbing potential has a spherical 3d-type symmetry. Using the two-dimensional wave functions of Eq. (1), the squares of the matrix elements for phonon scattering are

$$|I_0|^2=|\langle\psi_0(\vec{\mathrm{R}})|e^{i\vec{\mathrm{Q}}\cdot\vec{\mathrm{R}}}|\psi_0(R)\rangle|^2 =\frac{b_0^6}{(b_0^2+q_z^2)^3}\delta(\vec{\mathrm{k}}-\vec{\mathrm{k}}'-\vec{\mathrm{q}}) , \tag{9}$$

where $\vec{\mathrm{Q}}=(\vec{\mathrm{q}},q_z)$ and $\vec{\mathrm{R}}=(\vec{r},z)$ for intrasubband scattering, and

$$|I_1|^2=|\langle\psi_1(\vec{\mathrm{R}})|e^{i\vec{\mathrm{Q}}\cdot\vec{\mathrm{R}}}|\psi_0(\vec{\mathrm{R}})\rangle|^2 =\frac{4A^2q_z^2}{(\alpha^2+q_z^2)^4}\delta(\vec{\mathrm{k}}-\vec{\mathrm{k}}'-\vec{\mathrm{q}}) , \tag{10}$$

where $\alpha=3B=(b_0+b_1)/2$ for intersubband scattering. The relaxation time for acoustic-phonon scattering is given by

$$\frac{1}{\tau_i^{0,1}}=\frac{1}{2\pi\hbar}\int_0^{2\pi}d\theta\int dq_z\int dq\,q\,C_i(1-\cos\theta)|I_{0,1}|^2\times\delta(E_0(\vec{\mathrm{k}})-E_{0,1}(\vec{\mathrm{k}}+\vec{\mathrm{q}})) , \tag{11}$$

where i refers to either deformation-potential or piezoelectric scattering, with

$$C_i=C_{\text{ac}}=\frac{D^2k_BT}{2C_l}$$

for the deformation-potential scattering, and

$$C_i=C_{\text{pe}}\frac{e^2k_BTP^2}{\epsilon_s(q^2+q_z^2)}$$

for piezoelectric scattering. θ is the angle between $\vec{\mathrm{k}}$ and $\vec{\mathrm{k}}+\vec{\mathrm{q}}$, D is the deformation-potential constant, P is the piezoelectric coefficient, and C_l is the longitudinal elastic constant.

According to Eq. (11), phonon scattering rates are linear functions of temperature. This dependence is valid only at temperatures satisfying the condition

$$T > \frac{\hbar u_l q}{k_B} , \tag{12}$$

where $\hbar u_{lq}$ is the acoustic-phonon energy. At lower temperatures (in our case for temperatures lower than ~ 5 K) only phonons with small wave vectors, q, can participate in the scattering. For this reason the scattering-rate decrease with decreasing temperatures is faster than linear. However, since at these low temperatures the major contribution to electron mobility comes from temperature-independent scattering processes, such as remote ionized-impurity scattering, the approximation used in Eq. (11) has a negligible effect on total electron mobility.

Standard integration of the Eq. (11) gives the following results for the relaxation times:

$$\frac{1}{\tau_{ac}^0} = \frac{3m^* D^2 k_B T b_0}{16\hbar^3 C_l} , \tag{13}$$

and

$$1/\tau_{ac}^1 = b_{eff}/\tau_{ac}^0 b_0 , \qquad b_{eff} = \frac{2}{3}\frac{A^2}{\alpha^5} . \tag{14}$$

For the piezoelectric scattering,

$$\frac{1}{\tau_{pe}^0} = \frac{e^2 k_B T P^2 m^* b_0^6}{2\pi\epsilon_s \hbar^3 k^2} I(k,b_0) \tag{15}$$

where

$$I(k,b_0) = \frac{3\pi(4k^2-b_0^2)^2 - 4kb_0(5b_0^2-8k^2)}{16b_0^5(4k^2-b_0^2)^2} - \frac{3}{16(4k^2-b_0^2)^2} \times \begin{cases} \dfrac{1}{(4k^2-b_0^2)^{1/2}} \ln\left[\dfrac{2k-(4k^2-b_0^2)^{1/2}}{2k+(4k^2-b_0^2)^{1/2}}\right] , & 2k > b_0 , \\ \dfrac{2}{(b_0^2-4k^2)^{1/2}} \arccos\left[\dfrac{4k^2}{b_0^2}\right] , & 2k \le b_0 , \end{cases}$$

and

$$\frac{1}{\tau_{pe}^1} = \frac{2A^2 e^2 k_B T P^2 m^*}{\epsilon_s \hbar^3 k} \int_{-\infty}^{\infty} \frac{q_z}{(k^2+q_z^2)(\alpha^2+q_z^2)^4} dq_z . \tag{16}$$

The scattering rates given by Eqs. (15) and (16) were obtained by adopting a three-dimensional average of anisotropic electron-piezoelectric phonon interaction potential. In the two-dimensional case this average depends on the crystallographic plane in which the electron gas is confined.[17,18] The relaxation time for intersubband scattering was obtained in an approximate manner. Since the wave vectors of electrons in the excited subband are much smaller than those in the ground subband, we have assumed that the wave-vector change can be approximated by $|\vec{k}_0 - \vec{k}_1| \approx |\vec{k}_0| = k_F$. This is a good approximation for the electron density N_s, which is not much larger than N_s^{crit}. Even for the highest electron-gas densities considered in this paper, occupation of the first excited state does not exceed 1.5×10^{11} cm^{-2}.

Both of the aforementioned scattering processes are elastic, and therefore the relaxation-time approximation could be used. However, polar-optical scattering in GaAs is highly inelastic, due to the large optical-phonon energy, $\hbar\omega_0 = 36$ meV. Therefore, a proper treatment of this mechanism in a two-dimensional formalism would necessitate the inclusion of all the excited subbands which are separated from the Fermi energy be less than the optical-phonon energy. The scattering rate is thus the sum of many intersubband and intrasubband scattering processes over a wide energy range. This will result in a smearing out of the features which are characteristic of confinement of electrons in a two-dimensional system,[18] including the electron-density distribution within the well. Therefore, it can be argued that the three-dimensional approach to polar-optical-phonon scattering is justifiable also for 2D EG. Accordingly, the optical-phonon limited mobility was approximated by the mobility calculated for bulk semiconductors.[27]

B. Alloy-disorder scattering

For MDH involving ternary compounds, the additional scattering due to alloy-disorder potential should be included. Two distinct types of heterostructures may be invisaged in which the 2D EG is confined either within the alloy, or within the compound semiconductor. In the latter case, alloy-disorder scattering affects only the electrons which have penetrated into the alloy. In the former case, practically all of the electrons are subject to alloy-disorder scattering. Since both deformation-potential acoustic and alloy-disorder scattering result from short-range potentials, there is a formal similarity between the

relaxation times in both cases. Thus for intrasubband scattering the relaxation time can be written as[28,29]

$$\frac{1}{\tau^{0,1}_{\text{alloy}}}=\frac{m^*x(1-x)\Omega\langle V\rangle^2}{\hbar^3}I^{0,1}_{\text{alloy}}\ , \tag{17}$$

where x is the mole-fraction composition of the ternary alloy, $\langle V\rangle$ is the alloy-disorder scattering parameter, and Ω is the unit-cell volume. For electrons within the alloy,

$$I^0_{\text{alloy}}=\int_0^\infty |\chi_0(z)|^4dz=\tfrac{3}{16}b_0\ , \tag{18}$$

$$I^1_{\text{alloy}}=\int_0^\infty |\chi_0(z)|^2|\chi_1(z)|^2dz=\tfrac{3}{16}b_{\text{eff}}\ , \tag{19}$$

with b_{eff} given by Eq. (14). However, for the 2D EG within the compound semiconductor,

$$I^0_{\text{alloy}}=\int_{-\infty}^0 |\chi'_0(z)|^4dz\ , \tag{20}$$

and

$$I^1_{\text{alloy}}=\int_{-\infty}^0 |\chi'_0(z)|^2|\chi'_1(z)|^2dz\ , \tag{21}$$

where

$$\chi'_{0,1}(z)=M_{0,1}\exp[(2m^*V_0/\hbar^2)^{1/2}z]\ \text{ for } z<0$$

is the part of the wave function for both ground (0) and first excited subband (1), which describes penetration of the electron gas into the alloy. For large parameter V_0, M_0, and M_1 can be approximately determined from the balance of the forces acting on electrons at the interface. Using the approach of Ref. 15, one obtains,

$$|M_0|^2\approx\frac{4\pi e^2}{\epsilon_sV_0}(\tfrac{1}{2}N_s+N_{\text{depl}})\ , \tag{22}$$

and

$$|M_1|^2\approx\frac{4\pi e^2}{\epsilon_sV_0}(gN_s+N_{\text{depl}})\ , \tag{23}$$

where

$$g=\left\{1-\frac{4A^2}{b_0(\alpha+b_0)^3}\left[\frac{6}{(\alpha+b_0)^2}+\frac{3}{(\alpha+b_0)b_0}+\frac{1}{b_0^2}-\frac{\alpha}{\alpha+b_0}\left[\frac{10}{(\alpha+b_0)^2}+\frac{4}{(\alpha+b_0)b_0}+\frac{1}{b_0^2}\right]\right]\right\}.$$

In our calculations the screening of acoustic-phonon and alloy-disorder scattering by free carriers was neglected. This effect certainly should be included for all long-range interactions such as electron—piezoelectric-acoustic-phonon interaction. However, it is not obvious whether the short-range potentials, such as alloy-disorder and deformation-potential acoustic, should be screened by free carriers. Most of the analyses of transport in three-dimensional electron gas have neglected this type of short-range potential screening.

C. Ionized impurity scattering

The scattering of electrons confined in a triangular well by a screened ionized-impurity potential was originally considered for silicon inversion layers.[12] The relaxation time for this scattering process can be written in the following general form:[15]

$$\frac{1}{\tau^{0,1}_{\text{ion}}}=\frac{2\pi e^4}{\hbar}\int_{-L}^\infty dzN_i(z)\int_0^{2\pi}d\theta\int\frac{dq}{q}\frac{(1-\cos\theta)}{\epsilon^2(q)}\delta(E_0(\vec{k})-E_{0,1}(\vec{k}+\vec{q}))|F^{0,1}(q,z)|^2\ , \tag{24}$$

where

$$F^{0,1}(q,z)=\int dz'\chi_0^*(z')\chi_{0,1}(z')\exp(-q|z-z'|)\ , \tag{25}$$

$$\epsilon(q)=\epsilon_s\left[1+\frac{q_s}{q}\right], \tag{26}$$

and q_s is the screening parameter defined in the Appendix. $L-d$ is the width of the depletion region in $S2$.

As an approximation for the dielectric function for intersubband scattering the dielectric function for ground subband was used. This approximation is expected to be good, as long as the occupation of the excited subband is small. The function $N_i(z)$ represents the impurity distribution in the heterostructure and is shown in Fig. 1(a). The integration over z can be divided into four integrals, corresponding to remote scattering from the doped region of the $S2$ semiconductor, $-L\le z<-d$ from the undoped spacer $(-d<z<0)$, from interface charges at $z=0$ and from background residual impurities in the undoped semiconductor $(z>0)$. The expressions for relaxation times due to all of these scattering processes are given in the Appendix.

As discussed in the preceding section, Eq. (6) gives the relationship between the 2D EG density in the well and the concentration of remote ionized impurities. Thus, the only unknown parameters are the densities of residual ionized impurities in the spacer, N_i^s, residual impurities in the well, N_i^b, and the charge localized at the interface, N_i^{int}. It should be noted, however, that the contribution of ionized impurities located within the spacer is negligible for densities lower than about 3×10^{15} cm^{-3}.

Another scattering mechanism which has been found to be important for silicon inversion layers is the surface- (or interface-) roughness scattering.[15] In the case of MDH, part of this scattering process is included in the alloy-disorder scattering. Furthermore, interfaces extremely flat (on an atomic scale) are obtainable by the state-of-the-art MBE, and thus, this scattering mechanism was excluded from the present calculations.

IV. MOBILITY CHARACTERISTICS OF MODULATION-DOPED HETEROSTRUCTURES

Lattice matching represents one of the most severe limitations on achieving high-quality MDH. To date, three semiconducting-alloy systems have been shown to be suitable for MDH, namely, GaAs-(Ga,Al)As, $In_{0.53}Ga_{0.47}As$-InP (Ref. 30), and $In_{0.53}Ga_{0.47}As$-$In_{0.48}Al_{0.52}As$.[31,32] In the first case, the 2D EG is primarily confined in the GaAs, whereas in the latter two cases the electrons are located within the $In_{0.53}Ga_{0.47}As$. In Table I all the parameters used to calculate the electron mobility are listed. The values of the effective masses given are somewhat higher than for the bulk material; this is commonly attributed to the nonparabolicity of the conduction band.[15] There is a large margin of uncertainty regarding the values of the alloy-disorder parameters. However, several studies on $Ga_{1-x}Al_xAs$ have estimated this parameter to lie in the range of 0.8—1.0 eV.[35,36] In the case of (Ga,In)As MDH, since alloy-disorder scattering dominates low-temperature scattering, we were able to determine this parameter by fitting the available experimental data[31] with our theoretical model.

The highest electron mobilities reported for MDH were obtained for the (Ga,Al)As-GaAs system[20,21] at low temperatures. In fact, most of the work on single-quantum-well MDH has been reported for this system.

A. Temperature dependence of mobility

A basic mobility characteristic of MDH, which reveals the importance of the different mechanisms, is temperature dependence of the electron mobility. In Figs. 2 and 3 the calculated electron mobilities in the range 1—300 K are given for (Ga,Al)As-GaAs together with experimental data of Refs. 21 and 20, respectively. The component mobilities are also presented. At high temperatures, polar-optical-phonon scattering is the dominant scattering mechanism; on the other hand, at low temperatures electron mobility is limited by deformation-potential acoustic and piezoelectric acoustic-phonon scattering, together with alloy-disorder scattering and ionized-impurity scattering. The equilibrium concentration of remote ionized impurities in the doped region of the semiconductor

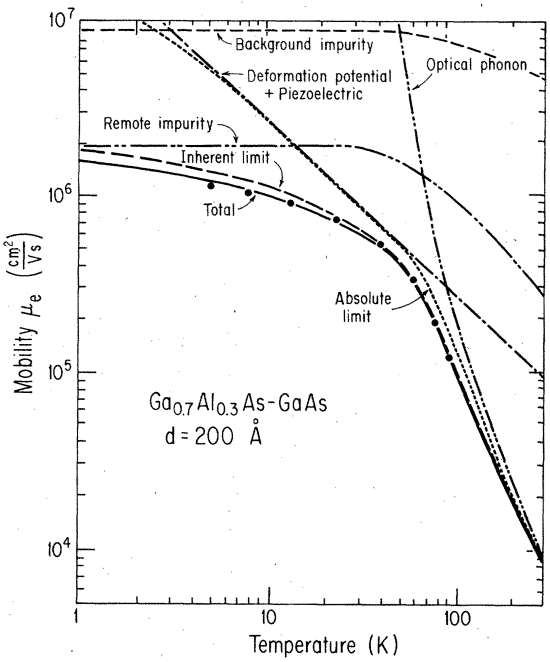

FIG. 2. Temperature dependence of the electron mobility in GaAs-$Ga_{1-x}Al_xAs$ heterostructures. Points are experimental data of Ref. 21 for a carrier density of 3×10^{11} cm^{-2}. The curves are calculated mobilities for this carrier density and a remote ionized-impurity concentration of 8.6×10^{16} cm^{-3}.

TABLE I. Parameters employed in present publication.

MDH	$Ga_{1-x}Al_xAs$-GaAs	$In_{0.53}Ga_{0.47}As$-$Al_{0.52}In_{0.48}As$
Parameter		
Electron effective mass m^*	$0.076m_0$[a]	$0.05m_0$[b]
Deformation potential D (eV)	7[c]	7[c]
Elastic constant c_l (dyn/cm^2)	13.97×10^{11}[c]	13.09×10^{11}[c]
Piezoelectric constant P	0.064[d]	0.034[c]
Static dielectric constant ϵ_0	12.9[c]	13.8[c]
High-frequency dielectric constant ϵ_∞	10.9[c]	10.3[c]
Optical-phonon energy $\hbar\omega_0$	36[c]	39.3[c]
Alloy-disorder parameter $\langle V\rangle$ (eV)	1[e]	0.63—0.55
Conduction-band energy offset V_0 (eV)	0.3[f]	0.53[g]

[a]Reference 33.
[b]Reference 31.
[c]Reference 26.
[d]Reference 34.
[e]Reference 35.
[f]Reference 15.
[g]Reference 30.

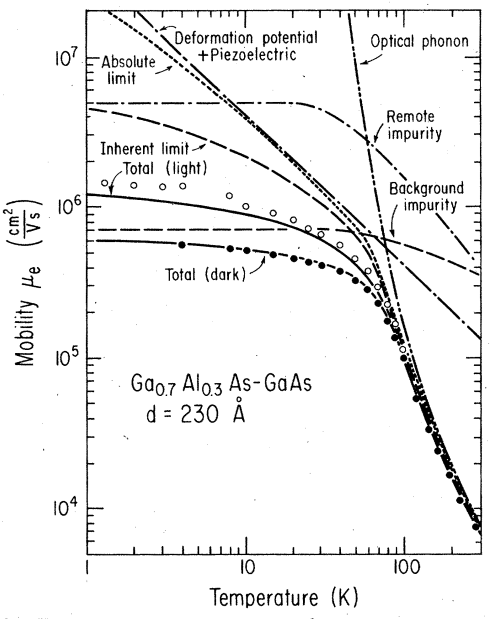

FIG. 3. Temperature dependence of the electron mobility in GaAs-$Ga_{1-x}Al_xAs$ heterostructure. The experimental data of Ref. 20 were obtained ● in the dark and ○ under illumination with $N_s=2.2\times10^{11}$ and 3.8×10^{11} cm^{-2}, respectively. The component mobilities given in the figure were calculated with $N_s=2.2\times10^{11}$ cm^{-2}.

$S2$ is related to the interface-electron density N_s and the spacer width d, by Eq. (6). Therefore, remote ionized-impurity scattering is always present in MDH. Thus, an "inherent limit" determined by alloy-disorder, phonon, and remote ionized-impurity scattering, exists for a given MDH. In Fig. 2 the inherent mobility limit saturates at low temperatures at about 1.8×10^6 $cm^2/V\,s$; the experimental data points of Ref. 21 lie very close to this limit; indicating that the other scattering mechanisms are not significant in this case. Similar values for ionized-impurity mobility limits were reported previously.[15,16] Slightly lower values of experimental mobility at low temperatures may be attributed to temperature-independent scattering processes. In fact, an excellent agreement is obtained when a small contribution from background ionized-impurity scattering at a concentration of 9×10^{13} cm^{-3} (which is very close to the ionized-impurity concentration one expects for "undoped" GaAs) is included. This result is a clear indication that additional scattering mechanisms such as surface-roughness and/or interface charge scattering are not appreciable in this case. Alloy disorder is also insignificant for such low electron densities. As seen in Fig. 1, these mechanisms become important at very low temperatures, where the phonon-limited mobility scattering is negligible. In the $T\rightarrow0$ K limit the absolute mobility limit is given by the alloy-disorder scattering.

In Fig. 3 experimental results of Ref. 20 for MDH with spacer width of 230 Å are given, together with the results of the theoretical calculations. The closed circles correspond to experimental data taken in the dark. These experimental mobilities are much lower than the inherent limit. To account for this discrepancy additional contributions are required from scattering by background impurity, interface charges and/or surface-roughness scattering. The higher mobility values (open circles in Fig. 3) correspond to data measured under illumination. As a result of the persistent photoconductivity effect, illumination increases the 2D EG density in the well from 2.2×10^{11} to about 3.8×10^{11} cm^{-2}. Taking this into account, we have calculated the total electron mobility both in the dark and under illumination, assuming additional contributions from background ionized impurities at the same level of 1×10^{15} cm^{-3}. Good agreement with experiment is seen in Fig. 3 at both electron densities. As discussed in Ref. 15, the surface-roughness scattering rate rapidly increases (corresponding mobility decreases) with increasing N_s; therefore, the observed mobility increase upon increase of N_s could not have been explained if surface-roughness scattering was important.

At very low temperatures the electron mobility saturates at a level determined by the alloy-disorder scattering which is $\sim10^8$ $cm^2/V\,s$ for $N_s=2.2\times10^{11}$ cm^{-2} and at $\sim4\times10^7$ $cm^2/V\,s$ for $N_s=3.8\times10^{11}$ cm^{-2}.

B. Electron density dependence of mobility

The 2D EG density may be continuously varied in MDH by external means: for example, illumination or gate voltage. Corresponding mobility changes are very pronounced, and they are of practical and fundamental importance. In Fig. 4 the calculated values of component mobilities of individual scattering processes are given as functions of N_s.[25] There are two reasons why these processes exhibit N_s dependences; first, direct dependence on the k vector, and second, dependence on the parameter b_0. For example, acoustic deformation-potential scattering mobility decreases with N_s solely due to the dependence of b_0 on N_s, derived using considerations of Sec. II. Alloy-disorder scattering exhibits the strongest N_s dependence, which originates from the enhanced penetration of the 2D EG into the alloy with increasing N_s [see Eqs. (22) and (23)].

The alloy-disorder mobility values in Fig. 4 are more than one order of magnitude greater than mobility calculated by Ando,[15] for the same MDH and using the same alloy-disorder potential. The reason for such a large discrepancy is not known at present; however, it certainly cannot be attributed to our approximate description of the penetration of the electron gas into the $Ga_{1-x}Al_xAs$. It should be emphasized that the present model is in agreement with calculations reported in Ref. 28. Using our formulas, we have calculated alloy-disorder mobility limited by scattering within the barrier of InP-$In_{1-x}Ga_xAs$, i.e., for the conditions similar to those outlined in Ref. 28(b). Adopting the same set of parameters we obtain $\mu_{alloy}\approx1.06\times10^8$ $cm^2/V\,s$ as compared with the value 9.5×10^7 $cm^2/V\,s$ of Ref. 28.

The increase of the experimental mobility seen in Fig. 4 with increasing N_s may be attributed to the presence of background and remote ionized impurities. The mobility due to these scattering mechanisms increases strongly with N_s. Accordingly, as seen in Fig. 4, for the MDH

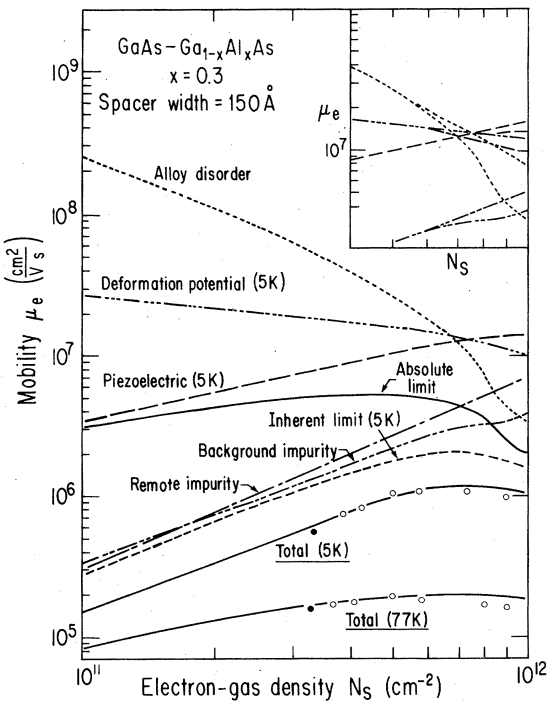

FIG. 4. Electron mobility at 5 and 77 K versus interface carrier density. Closed and open circles correspond to the experimental data of Ref. 21 measured in the dark and under illumination, respectively. Theoretical mobilities were calculated using remote and background ionized-impurity concentrations of 8.8×10^{16} and 1×10^{15} cm^{-3}, respectively. The critical concentration is 8×10^{11} cm^{-3} corresponding to $N_{\rm depl}=5\times10^{10}$ cm^{-2}. The inset shows the effect of intersubband scattering. The upper curves correspond to the intrasubband mobility, while the lower curves include the effect of the intersubband scattering with the broadening parameter $\Gamma=0.5$.

with the spacer width $d=150$ Å, the ionized-impurity electron mobility can be expressed in the form $\mu\sim N_s^{\gamma}$ with $\gamma=1.4$ and 1.2 for remote and background impurity scattering, respectively.

At higher N_s, values ($>7\times10^{11}$ cm^2), effects of intersubband scattering are important. They result in a lowering of the electron mobility compared with simple intrasubband scattering, as seen in the inset of Fig. 4. The most pronounced drop in the electron mobility is obtained for alloy-disorder scattering; this may be attributed to the large overlap of the parts of the electron wave functions for ground (0) and (1) states, which describe penetration of the 2D EG into the $Ga_{1-x}Al_xAs$. On the other hand, intersubband scattering for remote ionized impurities at finite spacer widths is negligible, owing to the exponential factor $\exp(-2\,|\vec{k}_0-\vec{k}_1|\,d)$ [see Eq. (A2)]. The combination of all the aforementioned scattering processes can provide an excellent explanation of the experimental data of Ref. 21, both at 5 and at 77 K. In the latter case optical phonons were included, with $\mu^{\rm opt}\sim6.5\times10^5$ cm^2/V s.

C. Spacer width dependence of mobility

The basic concept of MDH is to separate the 2D EG from parent ionized donors, thereby limiting ionized-impurity scattering from these remote centers. This consideration would dictate maximizing the spacer width, d, to maximize the mobility. However, according to Eq. (6) an increase of d leads to a decrease in the 2D EG density in the well, which has a deleterious effect on the electron mobility.

Importance of high N_s is highlighted in device applications of MDH, where one is more concerned with maximizing the channel conductivity ($\sigma_{\rm ch}=eN_s\mu_e$) rather than just the mobility values. Figure 5 gives the calculated component electron mobilities evaluated at maximum conductivities as a function of d.[25]

The inherent mobility limit increases rapidly with increasing spacer width, reaching mobilities of about 2×10^6 cm^2/V s at large spacer widths (>350 Å). The introduction of 1×10^{15} cm^{-3} background ionized impurities significantly alters this dependence, resulting in a peak mobility at $d\approx160$ Å. Higher background impurity concentrations shift the peak mobility to successively lower d values. The background concentration as a function of d at which the electron mobility attains its maximum value is given in Fig. 6; for MDH exhibiting high mobility, the maximum shifts to very large spacer widths. This behavior can qualitatively explain the reported mobility dependences on spacer width given in the literature; it has been found that in very high mobility MDH the mobility increases continuously with d,[20,21] whereas it has a distinct maxima for lower mobility MDH.[37]

In Fig. 7 the maximum inherent conductivity $\sigma_{\rm inh}^{\rm max}$

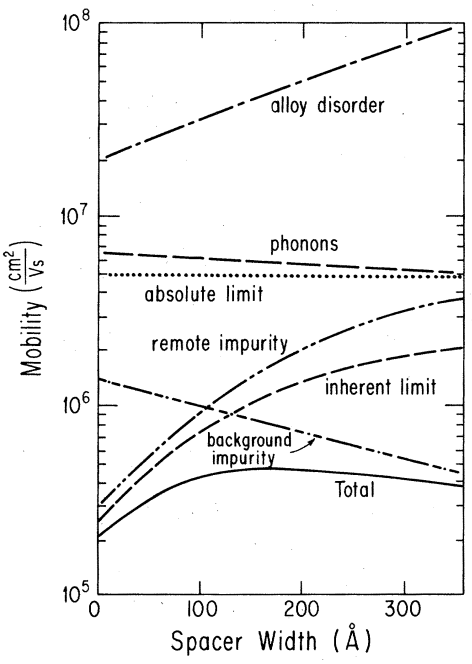

FIG. 5. Electron mobility values at maximum conductivity ($eN_s\mu_e$) versus spacer width for GaAs-$Ga_{0.7}Al_{0.3}As$ at 5 K. The "total" curve corresponds to a background impurity concentration $N_i^b=1\times10^{15}$ cm^{-3}.

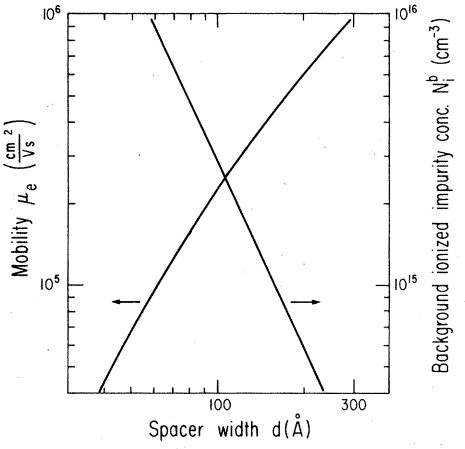

FIG. 6. Background ionized-impurity concentration and mobility for GaAs-$Ga_{0.7}Al_{0.3}As$ as a function of spacer width at which mobility attains its maximum value.

(maximized with respect to N_s at a given d), is plotted versus spacer width. Also, the N_s and N_i^r values required to maximum σ_{inh} are given in this figure. The ionized-impurity scattering is very sensitive to the distribution of ionized impurities and is therefore altered by smearing out the doping profile resulting from diffusion of impurities into the spacer, or even the well. This would have an especially profound effect at small spacer widths. However, it should be negligible for MDH with larger spacers exhibiting higher electron mobilities.

D. $In_{1-x}Ga_xAs$-based MDH

MDH based on $In_{0.53}Ga_{0.47}As$, and lattice matched to either InP (Ref. 30) or $Al_{0.52}In_{0.48}As$ (Ref. 31) have recently attracted a lot of interest. In these structures, the 2D EG is confined within the ternary compound $In_{1-x}Ga_xAs$ rather than on a binary system (GaAs) discussed above; therefore, it has been soon realized[28,29] that alloy-disorder scattering should play a much more prominent role. We have applied our model to the $In_{0.53}Ga_{0.47}As$-$Al_{0.52}In_{0.48}As$ MDH.

Figure 8 gives the total electron mobility, calculated as a function of temperature using the parameters listed in Table I, and compared with the experimental data of Ref. 31. As stated in Ref. 31, for $N_s > 4.5\times10^{11}$ cm^{-2}, the first excited band is already occupied, and thus intersubband scattering should be included. We have calculated the electron mobility including both intrasubband and intersubband scattering processes. It should be noted that our results for the intrasubband alloy-disorder scattering are in very good agreement with calculations of Ref. 28 where only the ground subband was considered. Inclusion of the intersubband scattering results in about 29% lower alloy-disorder mobility. Background impurity scattering was calculated using the limits for the background ionized-impurity concentration given in Ref. 31 [$N_i^b = (0.5 \text{ to } 1)\times10^{16}$ cm^{-3})]. By fitting the calculated mobilities to the experimental values at low temperatures, we were able to determine the alloy-disorder scattering parameter in this system. This determination is believed to be very accurate, as alloy scattering is the primary scattering mechanism limiting the electron mobility. Within this range of background impurity concentration, we have determined this parameter to be in the range 0.55—0.63 eV, which compares favorably with the bulk value of 0.60 eV as determined in Ref. 38.

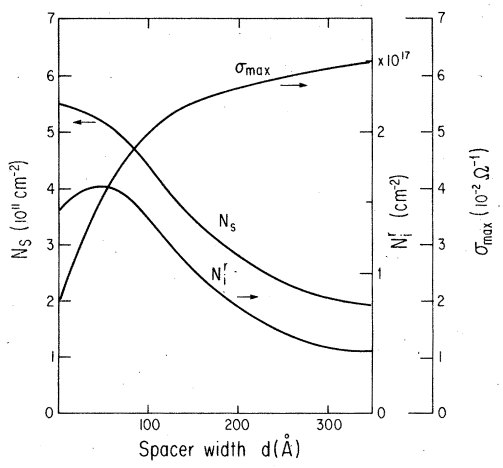

FIG. 7. Maximum inherent channel conductivity (maximized with respect to the charge density) as a function of the spacer width. The corresponding charge density and remote ionized-impurity concentration are also given in the figure.

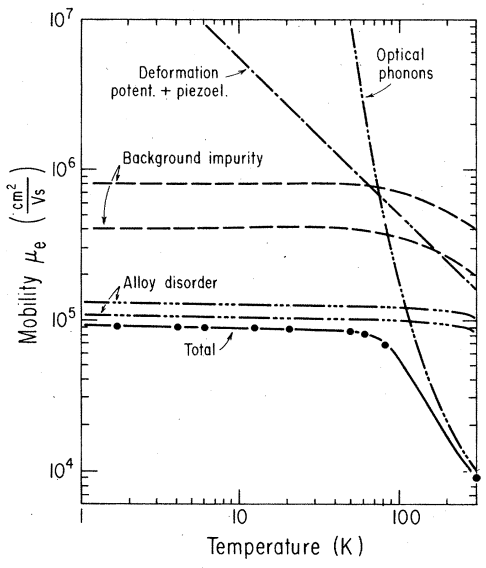

FIG. 8. Electron mobility is $In_{0.53}Ga_{0.47}As$-$Al_{0.52}In_{0.48}As$ with 80-Å spacer width. Experimental data points are from Ref. 31. The theoretical mobility was calculated for N_s taken from Ref. 31 with $N_s^{crit} = 4.5\times10^{11}$ cm^{-2} and $N_{depl} = 0$. The upper and lower background ionized-impurity limited mobilities correspond to $N_i^b = 0.5\times10^{16}$ and 1×10^{16} cm^{16}, respectively. Alloy-disorder scattering potential was used as a fitting parameter.

In the case of $In_{1-x}Ga_xAs$-$Ga_{1-y}Al_yAs$ MDH, one may expect a different electron-mobility dependence on N_s compared to GaAs-$Ga_{1-y}Al_yAs$ MDH. This originates from the opposite dependence of the electron mobility on N_s for alloy-disorder scattering as contrasted with ionized-impurity scattering. N_s dependence can therefore provide information about the relative contribution of alloy-disorder scattering to the total mobility.

There are two major factors affecting accuracy of the present calculations: first, the approximations used in the calculations of the electronic structure; second, the approximations used for the description of some of the scattering mechanisms. In the former case the accuracy of the present calculations depends solely on the accuracy with which parameter b_0 is determined. Comparing our results for remote ionized-impurity scattering with those of Ref. 15 based on self-consistent calculations of energetic structure, we conclude that the present calculations give mobilities $\sim 20\%$ higher at low electron densities (10^{11} cm^{-2}) and agree very well with the results of Ref. 15 at high electron densities (10^{12} cm^{-2}).

Another source of errors in the present calculations could be our approximate description of piezoelectric phonon scattering. We have found that the piezoelectric phonon-limited mobility calculated according to Eq. (15) is in good agreement with the calculations of Ref. 22 based on expressions obtained by two-dimensional averaging of unscreened electron-piezoelectric phonon interactions. Since the screening by free carriers will decrease the efficiency of the scattering, the present results can be treated as a lower limit for the piezoelectric phonon mobility. It should be noted, however, that piezoelectric phonon scattering contribution to the total mobility is important only in a very limited temperature range (20–60 K). Accordingly, it will not affect significantly the results for the total mobility.

V. SUMMARY AND CONCLUSIONS

In conclusion, we have presented a model for electron-mobility calculations which is directly applicable to single-quantum-well modulation-doped heterostructures. In this model a triangular well approximation for the confinement potential was used. All the major scattering processes were included, considering both intrasubband and intersubband transitions. Within the limitations pointed out above, we described the electron mobility over a broad range of temperatures (1–300 K) and electron densities (10^{11}–10^{12} cm^{-2}).

These calculations provided limits on the electron mobilities that are attainable in various semiconducting systems. In GaAs-$Ga_{1-x}Al_xAs$ heterostructures the inherent mobility limit increases with decreasing temperatures, reaching at very low temperatures a limit of about 2×10^6 for $x=0.3$ and at large spacer widths. On the other hand, for $In_{0.53}Ga_{0.47}As$-based heterostructures, alloy-disorder scattering limits the mobility to a level ($\sim 10^5$ cm^2/V s) at temperatures below 60 K. An accurate determination of alloy-disorder scattering potential parameter, $\langle V\rangle$, for $In_{1-x}Ga_xAs$ mixed crystals was therefore made. For both semiconducting systems considered, at temperatures above 60 K, optical phonons begin to limit the mobility. Furthermore, we have analyzed the effect of spacer width in optimizing channel-electron conductivity. Our results show that for the highest quality heterostructures maximum channel conductivity is only achieved at very large spacer widths, whereas for heterostructures exhibiting mobilities well below the inherent limit, an optimum spacer width is predicted.

ACKNOWLEDGMENTS

The authors are grateful to the U. S. National Aeronautics and Space Administration for financial support.

APPENDIX

The integration in Eq. (24) for the ionized-impurity scattering rate can be divided into four integrals, corresponding to regions of different ionized-impurity concentration: (1) remote ionized-impurity scattering from the heavily doped region, $z<-d$, with $N_i(z)=N_i^r$; (2) remote ionized-impurity scattering from the ions located within the spacer $-d<z<0$ with $N_i(z)=N_i^s$. Scattering rates from the ions in both of the above-mentioned regions can be expressed in the form

$$\frac{1}{\tau^0_{r,s}}=C_0\frac{b_0^6}{k^2}\int_0^{2k}\frac{[N_i^s(1-e^{-2qd})+N_i^r(e^{-2qd}-e^{-2qL})]}{P_0(q,b_0)(4k^2-q^2)^{1/2}}dq \tag{A1}$$

for intrasubband scattering and

$$\frac{1}{\tau^1_{r,s}}=C_1P_1(k_F,\alpha)[N_i^s(1-e^{-2k_Fd}) +N_i^r(e^{-2k_Fd}-e^{-2_FL})] \tag{A2}$$

for intersubband scattering, where

$$C_0=\frac{128\pi m^*e^4}{\hbar^3\epsilon_s^2},\quad C_1=\frac{2\pi^2m^*e^4}{\hbar^3\epsilon_s^2},\quad \alpha=(b_0+b_1)/2,\quad P_0(q,b_0)=[8q(q+b_0)^3+q_s(8b_0^3+9b_0^2q+3b_0q^2)]^2,$$

$$P_1(k,\alpha)=\frac{A^2(\alpha+2k)^2}{(k+q_s)^2(k+\alpha)^8k},$$

and

$$q_s=\frac{2\pi e^2}{\epsilon_s}\frac{N_s}{k_BT}\left\{\left[1+\exp\left[-\frac{E_F}{k_BT}\right]\right]\ln\left[1+\exp\left[\frac{E_F}{k_BT}\right]\right]\right\}^{-1}$$

is the inverse screening length.[14] The relaxation times for remote ionized-impurity scattering depend on the depletion layer width L. We have found, however, that for the cases considered in the present paper $-L$ can be replaced by $-\infty$. The error introduced by this approximation is about $\sim e^{-2q(L-d)}$ where $(L-d)=N_s/N_i^r>2.5\times10^{-6}$ cm. Thus, for the average momentum transfer $q=k_F\simeq2\times10^6$ cm^{-1} the error is less than 1%. The insensitivity of the remote impurity scattering to the depletion layer width was also reported in Ref. 15. Also, as seen from Eq. (A2), the intersubband scattering rate due to remote ionized-impurity scattering depends on the exponential factor $\exp(-2k_Fd)$ which becomes very small at large spacer width, d. Scattering from charges located at the interface with $N_i(z)=N_i^{\rm int}\delta(z)$ gives an inverse relaxation time of the form

$$\frac{1}{\tau_{\rm int}^0}=2C_0\frac{b_0^6N_i^{\rm int}}{k^2}\int_0^{2k}\frac{q^2dq}{P_0(q,b_0)(4k^2-q^2)^{1/2}} \tag{A3}$$

for intrasubband scattering and

$$\frac{1}{\tau_{\rm int}^1}=2C_1P_1(k_F,\alpha)k_FN_i^{\rm int} \tag{A4}$$

for intersubband scattering. Although the concentration of residual background ionized impurities is typically very small, their proximity to the 2D EG results in very effective electron scattering. The scattering rates for intrasubband and intersubband scattering are, respectively,

$$\frac{1}{\tau_{\rm int}^0}=2C_0\frac{b_0^6N_i^{\rm int}}{k^2}\int_0^{2k}\frac{q^2dq}{P_0(q,b_0)(4k^2-q^2)^{1/2}} \tag{A3}$$

where

$$F(x)=\frac{69-336x+630x^2-580x^3+264x^4-48x^5}{[32(1-2x)(1-x)^3+\beta(10-15x+6x^2)]^2},$$

$$x_k=\frac{k}{b_0},\quad \beta=\frac{q_s}{b_0},$$

and

$$\frac{1}{\tau_b^1}=C_1\frac{8A^2N_i^b}{(k_F+q_s)^2}\left[\frac{C(k_F)^2}{2k_F}-2C(k_F)R(k_F)+T(k_F)\right], \tag{A6}$$

where

$$C(k)=1-\frac{3B}{\alpha-k},$$

$$R(k)=\frac{a_0}{\alpha-k}+\frac{a_1}{(\alpha+k)^2}+\frac{2a_2}{(\alpha+k)^3}+\frac{6a_3}{(\alpha+k)},$$

$$T(k)=\frac{a_0}{2\alpha}+\frac{a_0a_1}{2\alpha^2}+\frac{a_1^2+2a_0a_0}{4\alpha^3}+\frac{3(a_0a_3+a_1a_2)}{4\alpha^4}+\frac{3(a_2^2+2a_1a_3)}{4\alpha^5}\frac{10a_2a_3}{\alpha^6}+\frac{45a_3^2}{8\alpha^7},$$

$$a_0=\frac{3B}{\alpha-k}+1-\frac{(\alpha-k)^3}{(\alpha+k)^3}+\frac{3B(\alpha-k)^3}{(\alpha+k)^4},$$

$$a_1=(\alpha-k)\left[1-\frac{(\alpha-k)^2}{(\alpha+k)^2}-\frac{3B}{\alpha-k}+\frac{3B(\alpha-k)^2}{(\alpha+k)^3}\right],$$

$$a_2=\frac{(\alpha-k)^2}{2}\left[1-\frac{\alpha-k}{\alpha+k}-\frac{3B}{\alpha-k}+\frac{3B(\alpha-k)}{(\alpha+k)^2}\right].$$

*Permanent address: Institute of Physics, Polish Academy of Sciences, AL. Lotniksow 32/46 02-668 Warsaw, Poland.

†Present address: University of Toronto, Downsview, Ontario, Canada M3H 5T6.

[1]L. Esaki and R. Tsu, IBM Research Laboratories, International Report No. RC 2418, 1969 (unpublished).

[2]R. Dingle, H. L. Störmer, A. C. Gossard, and W. Wiegmann, Appl. Phys. Lett. **33**, 665 (1978).

[3]S. Hiyamizu, T. Mimura, T. Fuji, K. Nanbu, and H. Hashimoto, Jpn. J. Appl. Phys. **20**, L245 (1981).

[4]T. J. Drummond, H. Morkoç, and A. Y. Cho, J. Appl. Phys. **52**, 1380 (1981).

[5]D. C. Tsui, A. C. Gossard, G. Kaminsky, and W. Wiegmann, Appl. Phys. Lett. **39**, 712 (1981).

[6]H. L. Störmer, A. C. Gossard, W. Wiegmann, and K. Baldwin, Appl. Phys. Lett. **39**, 912 (1981).

[7]K. Y. Cheng, A. Y. Cho, T. J. Drummond, and H. Morkoç, Appl. Phys. Lett. **40**, 147 (1982).

[8]S. Mori and T. Ando, Surf. Sci. **98**, 101 (1980).

[9]K. Hess, Appl. Phys. Lett. **35**, 484 (1979).

[10]B. K. Ridley, J. Phys. C **15**, 5899 (1982).

[11]J. Lee, H. N. Spector, and V. K. Arora, Appl. Phys. Lett. **42**, 363 (1983).

[12]F. Stern and W. Howard, Phys. Rev. **163**, 816 (1967).

[13]F. F. Fang and W. E. Howard, Phys. Rev. Lett. **16**, 797 (1966).

[14]T. Ando, A. B. Fowler, and F. Stern, Rev. Mod. Phys. **54**, 437 (1982).

[15]T. Ando, J. Phys. Soc. Jpn. **51**, 3900 (1982).

[16]F. Stern, Appl. Phys. Lett. **43**, 974 (1983).

[17]P. J. Price, Ann. Phys. (N.Y.) **133**, 217 (1981).

[18]P. J. Price, Surf. Sci. **113**, 199 (1982).

[19]P. K. Basu and B. R. Nag, Phys. Rev. B **22**, 4849 (1980).

[20]J. V. DiLorenzo, R. Dingle, M. Feuer, A. C. Gossard, R. Hendel, J. C. M. Hwang, A. Kastalsky, V. G. Keramides, R. A. Kelhl, and P. O'Connor, Int. Electron Device Meeting Tech Dig. **25**, 578 (1982).

[21]S. Hiyamizu, J. Saito, K. Nanbu, and T. Ishikawa, Jpn. J. Appl. Phys. **22**, L609 (1983).

[22]K. Lee, M. S. Shur, T. J. Drummond and H. Morkoc, J. Appl. Phys. **54**, 6432 (1983).

[23]H. L. Störmer, A. C. Gossard, and W. Wiegmann, Solid State Commun. **41**, 707 (1982).

[24]The intersubband scattering for Si inversion layers was considered by S. Mori and T. Ando, Phys. Rev. B **19**, 6433 (1979).

[25]W. Walukiewicz, H. E. Ruda, J. Lagowski, and H. C. Gatos, Phys. Rev. B **29**, 4818 (1984).

[26]See, for example, D. L. Rode, in *Semiconductors and Semimetals,* edited by R. K. Willardson and A. C. Beer (Academic, New York, 1975), Vol. 10, Chap 1.
[27]W. Walukiewicz, J. Lagowski, L. Jastrzebski, M. Lichtensteiger, and H. C. Gatos, J. Appl. Phys. **50**, 899 (1979).
[28](a) G. Bastard, Appl. Phys. Lett. **43**, 591 (1983); (b) see Ref. 9 of this reference.
[29]P. K. Basu and B. R. Nag, Appl. Phys. Lett. **43**, 689 (1983).
[30]Y. Guldner, J. P. Vieren, P. Voisin, M. Voos, M. Razeghi, and M. A. Poisson, Appl. Phys. Lett. **40**, 877 (1982).
[31]A. Kastalsky, R. Dingle, K. Y. Cheng, and A. Y. Cho, Appl. Phys. Lett **41**, 274 (1982).
[32]K. Y. Cheng, A. Y. Cho, T. J. Drummond, and H. Morkoç, Appl. Phys. Lett. **40**, 147 (1982).
[33]H. L. Störmer, A. Dingle, A. C. Gossard, W. Wiegmann, and M. D. Sturge, Solid State Commun. **29**, 705 (1979).
[34]J. S. Blakemore, J. Appl. Phys. **53**, R123 (1982).
[35]D. J. Chadi and M. L. Cohen, Phys. Status Solidi B **68**, 405 (1975).
[36]K. Masu, E. Tokumitsu, M. Konagai, and K. Takahashi, J. Appl. Phys. **54**, 5788 (1983).
[37]T. J. Drummond, H. Morkoç, and A. Y. Cho, J. Appl. Phys. **52**, 1380 (1981).
[38]J. R. Hayes, A. R. Adams, and P. D. Greene, in *GaInAsP Alloy Semiconductors,* edited by T. P. Pearsall (Wiley, New York, 1982).